29. C. J. Henry Dunand *et al.*, *J. Clin. Invest.* **125**, 1255–1268 (2015).
30. J. Mossong *et al.*, *PLOS Med.* **5**, e74 (2008).
31. J. M. Read *et al.*, *Proc. Biol. Sci.* **281**, 20140268 (2014).
32. P. Horby *et al.*, *PLOS ONE* **6**, e16965 (2011).
33. C. C. Dauer, R. E. Serfling, *Am. Rev. Respir. Dis.* **83**, 15–28 (1961).
34. L. Simonsen, T. A. Reichert, M. A. Miller, *Int. Congr. Ser.* **1263**, 791–794 (2004).

ACKNOWLEDGMENTS

We thank the Lloyd-Smith lab and the Worobey lab for helpful comments, C. Viboud for providing insight into historic influenza data, T. Mega and S. Wu for assistance compiling data, B. Cowling for sharing poultry exposure data, and P. Horby for sharing Vietnam contact data. K.M.G. is supported by the National Institute of General Medical Sciences of the National Institutes of Health (T32GM008185). M.A. is supported by the National Science Foundation Graduate Research Fellowship (DGE-1144087). M.W. is supported by the David and Lucile Packard Foundation. J.O.L-S. is supported by the National Science Foundation (EF-0928690); the Research and Policy for Infectious Disease Dynamics (RAPIDD) program of the Science and Technology Directorate, Department of Homeland Security; and Fogarty International Center, National Institutes of Health. The content is solely the responsibility of the authors and does not necessarily represent the official views of the National Institutes of Health. The authors declare no competing financial interests. Case data and code for model fitting are available as supplementary data files. Requests for materials should be addressed to M.W. or J.O.L.-S.

SUPPLEMENTARY MATERIALS

www.sciencemag.org/content/354/6313/722/suppl/DC1
Materials and Methods
Supplementary Text
Figs. S1 to S12
Tables S1 to S4
Database S1
References (*35*–*75*)

14 May 2016; accepted 3 October 2016
10.1126/science.aag1322

REPORTS

NANOPHOTONICS

Single-molecule optomechanics in "picocavities"

Felix Benz,[1] Mikolaj K. Schmidt,[2] Alexander Dreismann,[1] Rohit Chikkaraddy,[1] Yao Zhang,[2] Angela Demetriadou,[2,3] Cloudy Carnegie,[1] Hamid Ohadi,[1] Bart de Nijs,[1] Ruben Esteban,[2] Javier Aizpurua,[2]* Jeremy J. Baumberg[1]*

Trapping light with noble metal nanostructures overcomes the diffraction limit and can confine light to volumes typically on the order of 30 cubic nanometers. We found that individual atomic features inside the gap of a plasmonic nanoassembly can localize light to volumes well below 1 cubic nanometer ("picocavities"), enabling optical experiments on the atomic scale. These atomic features are dynamically formed and disassembled by laser irradiation. Although unstable at room temperature, picocavities can be stabilized at cryogenic temperatures, allowing single atomic cavities to be probed for many minutes. Unlike traditional optomechanical resonators, such extreme optical confinement yields a factor of 10^6 enhancement of optomechanical coupling between the picocavity field and vibrations of individual molecular bonds. This work sets the basis for developing nanoscale nonlinear quantum optics on the single-molecule level.

Coinage metal nanostructures support localized surface plasmons, which confine optical fields to much smaller than their wavelength (*1*). This extreme enhancement enables vibrational spectroscopy within small volumes, even down to single molecules (*2*, *3*). For many years, lateral resolution was believed to be ~10 nm (*4*); however, recent experiments have resolved the atomic structure of single molecules using tip-enhanced Raman spectroscopy (TERS) (*3*) and have demonstrated direct sequencing of RNA strands (*5*). Atomistic simulations also suggest that plasmonic confinement to atomic scales is possible (*6*).

Here, we show that light-activated mobilization of surface atoms in a plasmonic hotspot triggers the formation of additional "picocavities" bounded by a single gold atom. Because of strong optical field gradients that switch the Raman selection rules, the ultrasmall localization of light in these cavities alters the number and variety of vibrational modes of trapped molecules observed. The resulting cascaded ultrastrong plasmonic confinement pumps specific molecular bonds, thereby creating nonthermal vibrational populations and constituting an optomechanical resonator. Remarkably, cryogenic control of the plasmonic nanometric cavity allows for systematic and stable monitoring of picocavity formation and disassembly. We thus demonstrate the possibility of resolving the dynamics of individual bonds within molecules. The existence, monitoring, and selective control of these picocavities will be important not only in photochemistry and photophysics but also as a platform for optomechanics, coherent control, and quantum information devices.

To produce stable, robust picocavities, we bypass complex scanning tip spectroscopies, instead using straightforward self-assembly to create "nanoparticle-on-mirror" (NPoM) geometries (Fig. 1A). Individual gold nanoparticles are spaced above a planar gold substrate by a nanometer-thick self-assembled monolayer (SAM) of biphenyl-4-thiol (Fig. 1B). Both the scattering and surface-enhanced Raman spectroscopy (SERS) signals from individual constructs are highly reproducible. All measurements are recorded at cryogenic temperatures, using a modified dark-field microscope and laser pumping at 633 nm (*7*). Low-temperature time-series SERS spectra from a typical gold nanoparticle (Fig. 1C) show vibrational modes that can be divided into two sets: A first set of vibrational modes is ever-present with constant intensity ("persistent lines") while a second "blinking" set of lines appears (arrows), disappears, and changes intensity over time.

Comparing the observed spectra with density functional theory (DFT) simulations confirms that both types of lines originate from the biphenyl-4-thiol SAM. However, in the blinking set, the relative intensities are altered, and normally Raman-inactive lines [infrared (IR) absorption lines] are mixed into the SERS spectrum. Each realization of this fluctuating state displays different lines for each enhancement, indicating selective excitation of specific vibrations (see fig. S13 for additional spectra). By contrast, SERS intensities in the persistent set are unaffected by the appearance of blinking lines. As shown below, this suggests that the blinking lines originate from a very small volume inside the plasmonic gap, containing only a single molecule. Such tight localization yields extremely high field gradients, accounting for the observation of Raman-inactive IR modes (*8*). Additional evidence implies that these small hotspots are actually sub-nm^3 volumes that we term "picocavities," each consisting of only one gold atom. Full electromagnetic simulations (Fig. 1, D and E) show that picocavities locally boost the near-field intensity, leaving the rest of the plasmonic hotspot unaffected. The high field intensity within the extremely small (<1 nm^3) local hotspot (Fig. 1, D and E) markedly enhances the SERS intensity of nearby molecules. We find that picocavities are spontaneously formed and destroyed under laser illumination but can be stabilized.

Picocavities are atomic-scale subnanometer structures forming an extreme class of optical localization that pushes electromagnetic coupling to the limit. To exploit and monitor their optical activity and to experimentally estimate the picocavity localization volume V_{loc}, we explore how they modify the Raman scattering when exciting a molecular vibration. This process is greatly amplified by the extreme confinement of the incident light in the plasmonic gap. As a result, the population n of excited vibrational states (at frequencies

[1]NanoPhotonics Centre, Cavendish Laboratory, Department of Physics, University of Cambridge, Cambridge CB3 0HE, UK. [2]Materials Physics Center CSIC-UPV/EHU and Donostia International Physics Center, 20018 Donostia–San Sebastián, Spain. [3]Blackett Laboratory, London SW7 2AZ, UK.
*Corresponding author. Email: jjb12@cam.ac.uk (J.J.B.); aizpurua@ehu.es (J.A.)

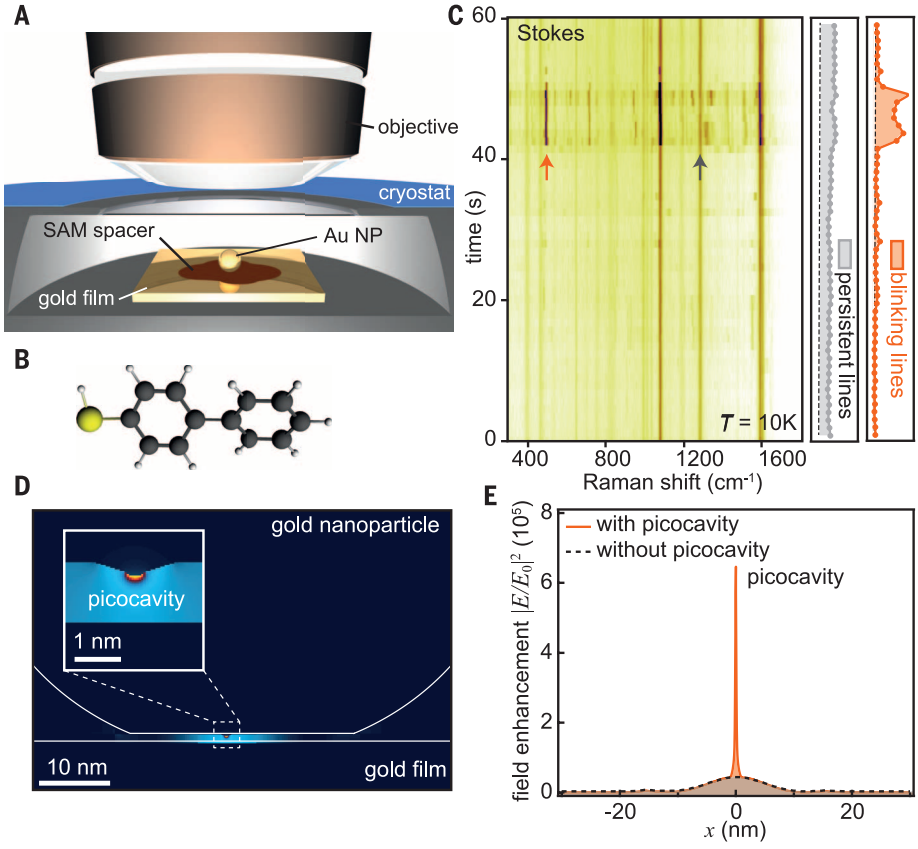

Fig. 1. Raman spectra from molecules in picocavities and near-field light distribution. (**A**) Schematic cooled nanoparticle-on-mirror (NPoM) geometry. (**B**) Biphenyl-4-thiol molecule in monolayer. (**C**) SERS time series from a single 90-nm NPoM with 60 μW/μm^2 pump (arrows correspond to persistent and blinking lines; see right). (**D** and **E**) Simulations of a faceted gold nanoparticle with and without atomic protrusion at x = 0 nm. (D) Near-field map. Inset is an enlarged view of the picocavity showing subnanometer localization of optical field. (E) Near-field intensity across the gap.

ω_m) is boosted above that provided by thermal excitations from the environment at temperature T,

$$n_{th} = \left[\exp\left(\frac{\hbar\omega_m}{k_B T}\right) - 1\right]^{-1} \quad (1)$$

by an additional contribution due to the optomechanical coupling of the plasmonic cavity with the molecular vibration (*9*), where $\hbar$ is the Planck constant divided by 2π and k_B is the Boltzmann constant. We first model the interaction of quantized plasmons with phonons in the classical limit of weak coupling strength g between the vibrations and cavity plasmons [with $g << (\omega_m, \kappa)$ for cavity decay rate κ] through the optomechanical Hamiltonian described in (*7*, *9*, *10*). This gives

$$n = \frac{\Gamma_{opt} n_{rad} + \Gamma_m n_{th}}{\Gamma_{opt} + \Gamma_m} \quad (2)$$

where $\Gamma_{opt}(V_{loc}) \propto g^2 I$ is the volume-dependent optomechanical amplification rate, which in turn depends on optomechanical coupling strength $g(V_{loc})$ and laser power I, and Γ_m is the phonon decay rate (*7*, *9*). At T = 10 K ($k_B T$ = 0.9 meV), population n_{th} can be neglected because vibrational energies ($\hbar\omega_m$ = 124 meV for 1000 cm^{-1}) greatly exceed thermal energies. Depending on the detuning of the laser from the cavity, Γ_{opt} can either be positive (damping the vibration) or negative (amplifying the vibration). For sufficiently high intensities or sufficiently strong coupling, amplification (Γ_{opt}) overcomes phonon decay (Γ_m), creating a nonthermal phonon population (dominating when $\Gamma_{opt} n_{rad} >> \Gamma_m n_{th}$). Experimentally measuring this vibrational state population at increasing laser power allows evaluation of the Raman localization volume V_{loc} (*7*).

In the regime of vibrational pumping, n can be quantified by simultaneously recording both the Stokes and anti-Stokes parts of the SERS spectrum and evaluating their ratio for each mode (*11*, *12*). The plasmon contribution to the population (arising from the quantum backaction mechanism) follows

$$n_{rad} = \left[4\omega_m(\omega_c - \omega_\ell)\mathcal{L}_-\right]^{-1} \quad (3)$$

where

$$\mathcal{L}_\pm = \left[(\omega_c - \omega_\ell \pm \omega_m)^2 + \left(\frac{\kappa}{2}\right)^2\right]^{-1} \quad (4)$$

is a Lorentzian profile of the field enhancement supported by the cavity resonance at frequency ω_c, illuminated by the laser with frequency ω_ℓ. The ratio of anti-Stokes to Stokes scattering is then

$$\frac{S(\omega_{aS})}{S(\omega_S)} \approx \left(\frac{\omega_\ell + \omega_m}{\omega_\ell - \omega_m}\right)^4 \frac{\mathcal{L}_-}{\mathcal{L}_+} \frac{n}{1+n} \quad (5)$$

Although the above analytic formalism is correct for coupling $g << \kappa$, corrections are needed from the full numerical solution of the underlying optomechanical Hamiltonian [see implementation in (*7*)] to properly extract estimates of the localization volume.

Low-temperature SERS shows that prominent anti-Stokes SERS lines blue-shifted from the laser (Fig. 2A) appear always and only when the additional fluctuating Stokes lines are present. Time-series SERS spectra (Fig. 2B) show that none of the persistent Stokes lines are seen in the anti-Stokes spectra (dashed lines), reflecting the low excited-state population at 10 K for most molecules within the NPoM gap but outside the picocavity. Taking the measured anti-Stokes/Stokes ratio, we use Eq. 5 in the thermal limit (setting $n = n_{th}$) to extract for each vibrational mode an effective temperature (marked in Fig. 2A), far exceeding the sample temperature (up to 2000 K for certain lines). These effective temperatures are different for each line and increase with increasing vibrational energy, thus providing clear proof that the vibrational populations are nonthermal and that the pumping contribution to the population cannot be ignored. Plasmons do not directly heat the molecules, as shown by the absence of characteristic anti-Stokes background signals, previously shown to track the temperature of metallic nanostructures (*13*); the gold remains cold throughout, as expected for these sub–100-μW optical powers.

In such time-series SERS scans, whenever the picocavity regime appears, spectral wandering of the vibrational energies of 0.1 to 1 cm^{-1} s^{-1} is seen (Fig. 2B), which is a typical signature of single-molecule SERS (*14*, *15*). This provides additional confirmation that the blinking lines come from a very small subregion of the NPoM gap containing individual molecules. Further proof comes from observation of IR-active lines, which arise from the strong field gradients around the picocavity that alter the SERS selection rules (*3*, *8*) and necessarily require field localization of <0.5 nm, consistent with picocavities in the nanogap. Theoretically, this effect can be reproduced by recalculating the SERS spectrum from the full Raman tensor (obtained by DFT) assuming only local illumination. Using a field localization of 0.4 nm, extracted from the picocavity field confinement lateral width (Fig. 1D), the observed experimental spectra (Fig. 2, C and D, bottom) can be modeled only when repositioning the picocavity relative to the molecule (Fig. 2, C and D, top; insets depict geometries used for each). To reproduce our experimental spectra, confinement on the order of a

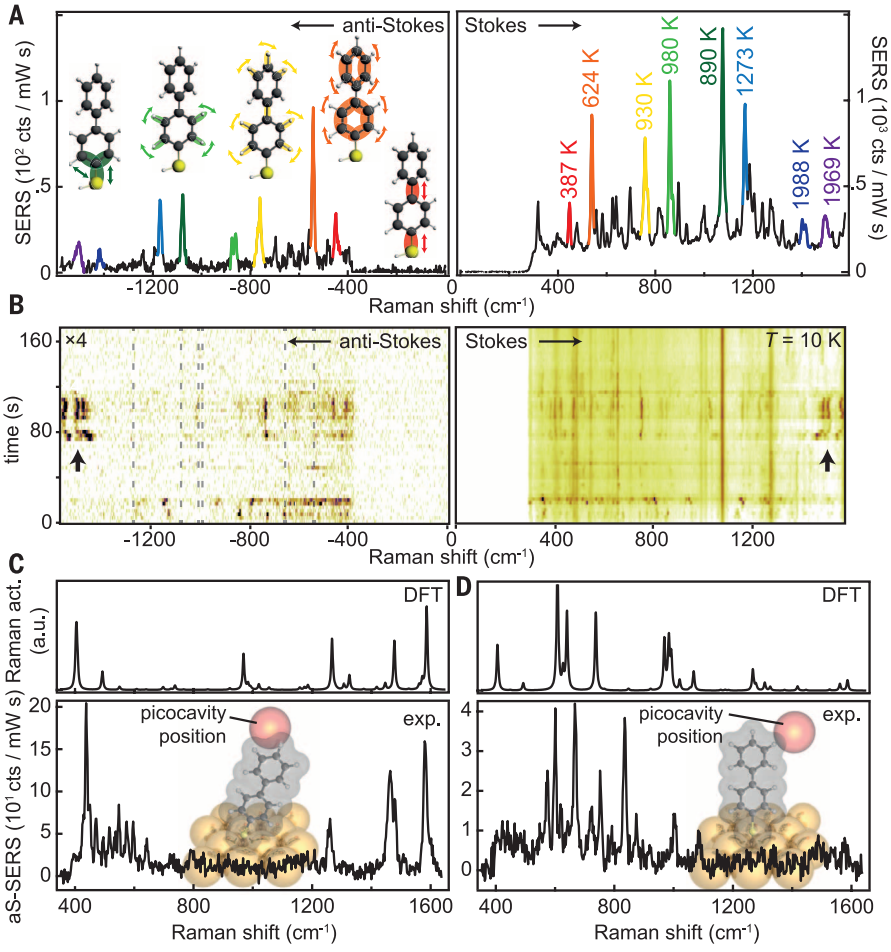

Fig. 2. Raman spectra reveal changes of SERS selection rules. (**A**) Anti-Stokes/Stokes spectra at a time when additional picocavity-induced lines are present. Colors correspond to same lines on Stokes and anti-Stokes sides, with vibrational eigenmodes and effective temperatures shown. (**B**) Time-series anti-Stokes and Stokes SERS. Dashed lines (aS) mark expected aS line positions corresponding to ever-present (persistent) S lines from the many molecules in the larger nanocavity. (**C** and **D**) Comparison of two experimental spectra (bottom) with DFT simulated spectra (top) under the assumption of atomic-scale field confinement (inset shows geometries; red sphere denotes field localization for simulations).

single gold atom is required (*7*), giving direct proof for the atomic confinement of the optical field. In this regime, individual bonds within molecules can be accessed.

Using our Raman formalism to extract V_{loc} requires confirmation that vibrational pumping dominates, for which a linear power dependence of the anti-Stokes/Stokes ratio is expected (*9*, *11*, *12*), as seen from Eq. 5 for small n. Previous investigations have encountered difficulty in stabilizing nanostructures while measuring such power dependences. We avoided this problem by modifying our experiments to identify in real time whenever blinking lines appear and then immediately cycling the laser power (Fig. 3A shows typical data). We thus repeatedly recorded anti-Stokes/Stokes ratios for different 633-nm laser powers. Extracting power series for several different lines (Fig. 3, B and C), recorded on different nanoparticles at different times, always gave a quadratic power dependence of the anti-Stokes signal and a linear power dependence for the anti-Stokes/Stokes ratio (and hence the phonon population), supporting the presence of vibrational pumping. However, the slope of these linear fits changed from mode to mode and also differed for different realizations on different nanoparticles. This suggests that the slope is a measure of picocavity geometry, which controls the different optomechanical coupling strengths of the molecular vibrations, because $g \propto 1/V_{loc}$.

From more than 50 picocavities, we observed coupling strengths $\hbar g$ = 5 to 40 meV (Fig. 3D), reaching $g/\kappa \sim 0.2$. From Eq. 2, such high coupling strengths [compared to <1 μeV for conventional optomechanical systems (*9*, *16*–*19*)] correspond to extremely small Raman localization volumes of <1 nm^3 (*7*). This extremely tight localization agrees with electromagnetic simulations using atomic-scale features in the gap region, also giving lateral localizations of ~0.23 nm [full width at half maximum (FWHM) of intensity; Fig. 1E], as well as with previous theory

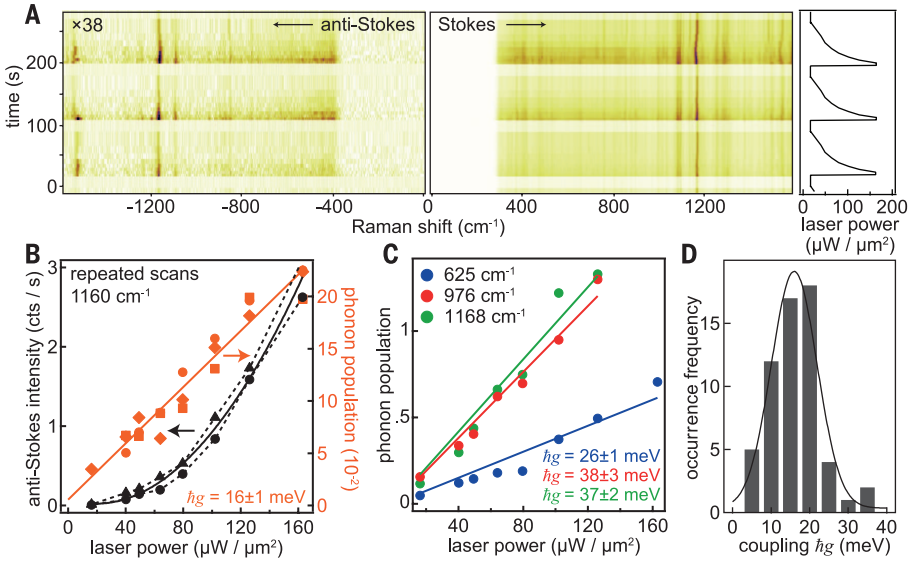

Fig. 3. Vibrational pumping of molecular vibrations in picocavities. (**A**) SERS time scan for varying laser power (shown on right). (**B**) Extracted laser power dependence of anti-Stokes intensity and phonon population for different measurements on the same picocavity. (**C**) Power dependence of phonon population for different vibrational modes in the same picocavity. (**D**) Distribution of observed optomechanical coupling strengths g.

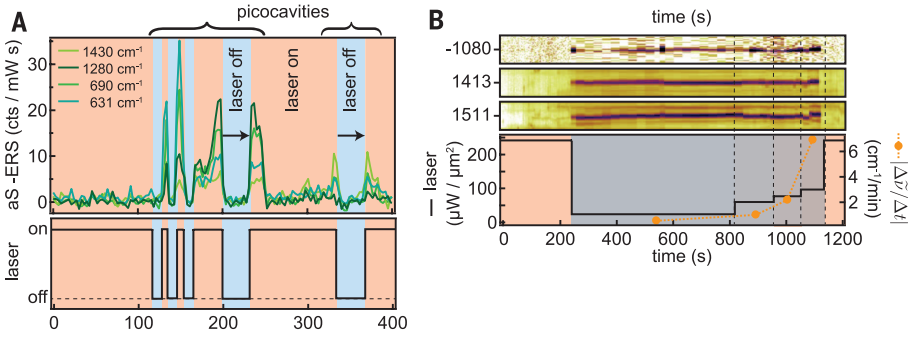

Fig. 4. Picocavity stability in the dark. (**A**) Anti-Stokes intensities as the laser (bottom) is switched on and off demonstrate the picocavity stability, which persists (arrows) without the laser. (**B**) Picocavities are also stable at low laser powers. Anti-Stokes intensities are observed as laser power is dropped by a factor of 10 when picocavity formation is detected. After waiting 10 min, the power is increased stepwise. SERS intensities are normalized by laser power. The lower graph shows the simultaneously measured rate of spectral wandering (orange) versus laser power.

predicting atomic-scale confinement of optical fields (*6*, *20*). This optical confinement explains atomic resolution in tip-based experiments (*3*, *5*) and approaches the quantum limit derived previously (*4*), $V \sim Rd_{QR}^2$, but with the radius of curvature R now set by the size of single atoms $R \sim 0.15$ nm and tunneling length scale $d_{QR} \sim 0.4$ nm, giving $V_{\min} \sim 10^{-2}$ nm^3. We highlight the strongly inhomogeneous distribution of the picocavity field within the plasmonic gap, resulting in a complex relationship between the Raman localization volume and standard quantum optical definitions of mode volume (*7*).

To account for both formation and disassembly of picocavities at cryogenic temperatures requires atomic surface reconstructions facilitated by irradiation. To demonstrate the dependence on laser power, we immediately switched off the laser once the formation of a picocavity was detected. After a delay time, varied between 3 and 30 s, the laser was switched on again (Fig. 4A), allowing us to examine whether the atomic configuration relaxes in the dark. In all cases, we found that the SERS spectra reappear with exactly the same strength as before the laser is switched off (see also fig. S14). This further proves that the additional strong Stokes and anti-Stokes SERS lines originate from a robust formation of these picocavities and cannot be attributed to heating of the molecules; for a process involving heating, one instead expects the system to cool back down once the laser is switched off.

Even when the laser power was reduced instead of being switched off, the lifetime of these picocavities was greatly extended (Fig. 4B), thus allowing continuous monitoring. A picocavity was easily stabilized for more than 10 min by reducing the laser power by a factor of 10 after cavity formation was observed. After 10 min at the lower laser power, the power was increased stepwise, and disassembly was observed at a laser power density of 100 μW/μm^2. Both formation and disassembly of the picocavity were abrupt (<1 s), whereas fluctuations of the vibrational energies were found to increase as the laser power increased. Hence, the fluctuation of the molecular vibrational energies is possibly driven by Au atom movement (see Fig. 4B and fig. S12).

Laser illumination not only destabilizes the picocavity atomic configurations but also is crucial in their formation. To demonstrate this, we recorded several time-series SERS scans for different laser powers and extracted the occurrence frequency of picocavity formation. We found a clear Arrhenius-type behavior with critical laser power density $P_c = 256 \pm 15$ μW/μm^2, corresponding to an energy of 0.7 eV (*7*). This energy is comparable to previously reported activation energies for gold adatom surface diffusion of 0.9 eV (*21*). Repeating the experiments using silver instead of gold, we observed a higher critical power density of $P_c = 388 \pm 48$ μW/μm^2 but otherwise similar behavior. We cannot yet identify whether this critical P_c corresponds to a characteristic thermal hopping barrier or to optical forces arising from the extreme field gradients around single-atom protrusions. However, we note that formation of a picocavity can be facilitated by the stability of gold-thiol "staples": Two thiols cooperatively pull a gold atom into an elevated position, forming a bridgelike arrangement [see (*22*) and references therein].

Our findings are also in line with observations that SERS blinking has both a thermal-activated and a light-activated component (*23*). Picocavities only appear in near-field–sensitive measurements such as SERS, whereas no changes are seen in far-field scattering that depend only on the properties of the larger hosting nanocavity. Our findings suggest that picocavities are omnipresent in SERS and TERS measurements on nanoscale plasmonic hotspots (such as colloidal aggregates, dimers, and NPoMs) and are responsible for single-molecule and atomic resolution that has been obtained. The extreme optical confinement yields selective amplification of molecular vibrations of only a few bonds within the single molecule isolated by each picocavity, presumably depending on the exact mutual configuration of Au atom protrusion and bound thiol orientation. Optical field strengths of 0.3 V/nm here may be further exploited.

Picocavities are stable at cryogenic temperatures but at room temperature are in constant dynamical creation and destruction. They form as a result of photon-assisted surface reconstruction of gold. Stabilizing these picocavities while probing them takes plasmonic-molecule coupling to the extreme and opens widespread possibilities for studying and exploiting light-molecule coupling—for instance, in molecular interactions, chemical reactions, superradiant emission, electron transfers, and single-molecule electrochemistry—and advances the fundamental access of light to the building blocks of matter.

REFERENCES AND NOTES

1. W. L. Barnes, A. Dereux, T. W. Ebbesen, *Nature* **424**, 824–830 (2003).
2. K. Kneipp *et al.*, *Phys. Rev. Lett.* **78**, 1667–1670 (1997).
3. R. Zhang *et al.*, *Nature* **498**, 82–86 (2013).
4. K. J. Savage *et al.*, *Nature* **491**, 574–577 (2012).
5. E. Bailo, V. Deckert, *Angew. Chem. Int. Ed.* **47**, 1658–1661 (2008).
6. M. Barbry *et al.*, *Nano Lett.* **15**, 3410–3419 (2015).
7. See supplementary materials on *Science* Online.
8. M. Moskovits, D. P. DiLella, K. J. Maynard, *Langmuir* **4**, 67–76 (1988).
9. M. K. Schmidt, R. Esteban, A. González-Tudela, G. Giedke, J. Aizpurua, *ACS Nano* **10**, 6291–6298 (2016).
10. P. Roelli, C. Galland, N. Piro, T. J. Kippenberg, *Nat. Nanotechnol.* **11**, 164–169 (2016).
11. R. C. Maher, C. M. Galloway, E. C. Le Ru, L. F. Cohen, P. G. Etchegoin, *Chem. Soc. Rev.* **37**, 965–979 (2008).
12. D. R. Ward, D. A. Corley, J. M. Tour, D. Natelson, *Nat. Nanotechnol.* **6**, 33–38 (2011).
13. J. T. Hugall, J. J. Baumberg, *Nano Lett.* **15**, 2600–2604 (2015).
14. S. Nie, S. R. Emory, *Science* **275**, 1102–1106 (1997).
15. C. C. Neacsu, J. Dreyer, N. Behr, M. B. Raschke, *Phys. Rev. B* **73**, 193406 (2006).
16. R. Esteban, T. V. Teperik, J. J. Greffet, *Phys. Rev. Lett.* **104**, 026802 (2010).
17. X. Zeng *et al.*, *Opt. Express* **22**, 14517–14523 (2014).
18. M. Liu, T.-W. Lee, S. K. Gray, P. Guyot-Sionnest, M. Pelton, *Phys. Rev. Lett.* **102**, 107401 (2009).
19. X.-W. Chen, M. Agio, V. Sandoghdar, *Phys. Rev. Lett.* **108**, 233001 (2012).
20. X. Chen, J. E. Moore, M. Zekarias, L. Jensen, *Nat. Commun.* **6**, 8921 (2015).
21. T.-S. Lin, Y.-W. Chung, *Surf. Sci.* **207**, 539–546 (1989).
22. T. Bürgi, *Nanoscale* **7**, 15553–15567 (2015).
23. S. R. Emory, R. A. Jensen, T. Wenda, M. Han, S. Nie, *Faraday Discuss.* **132**, 249–259 (2006).

ACKNOWLEDGMENTS

Supported by Project FIS2013-41184-P from MINECO (Ministerio de Economía y Competitividad) and IT756-13 from the Basque government consolidated groups (M.K.S., Y.Z., A. Demetriadou, R.E., and J.A.); the Winton Programme for the Physics of Sustainability (F.B.); the Dr. Manmohan Singh scholarship from St. John's College (R.C.); the UK National Physical Laboratory (C.C.); the Fellows Gipuzkoa Program of the Gipuzkoako Foru Aldundia via FEDER funds of the European Union "Una manera de hacer Europa" (R.E.); UK Engineering and Physical Sciences Research Council grants EP/G060649/1 and EP/L027151/1; and European Research Council grant LINASS 320503. Source data can be found at DOI: 10.17863/CAM.1675.

SUPPLEMENTARY MATERIALS

www.sciencemag.org/content/354/6313/726/suppl/DC1
Materials and Methods
Figs. S1 to S16
References (*24*–*35*)

11 July 2016; accepted 30 September 2016
10.1126/science.aah5243